Applied Physics B (2019) 125:212
https://doi.org/10.1007/s00340-019-7326-5

Applied Physics B
Lasers and Optics

Electro-optic sensor for static fields

J. O. Grasdijk[1,2,6] · X. F. Bai[1,2] · I. Engin[5] · K. Jungmann[1,2] · H. J. Krause[5] · B. Niederländer[4] · A. Offenhäuser[5] · M. Repetto[4] · L. Willmann[1,2] · S. Zimmer[3,4]

Received: 11 July 2019 / Accepted: 4 October 2019

Abstract
A sensor has been developed for low frequency and DC electric fields E. The device is capable of measuring fields with ΔE = 4 (1) V/cm resolution. It is based on a Y-cut Z-propagation lithium niobate electro-optic crystal. For a particular commercially available bare crystal, we achieved an in air time constant $\tau_c(air) = 6.4(1.8)$ h for the decay of the electro-optic signal. This enables field monitoring for several hours. As an application, we demonstrated that a constant electric field $E^{ext} = 640$ V/cm applied via external electrodes to a particular spherical glass container holding an Xe/He gas mixture decays inside this cell with a time constant $\tau_E^{glass} = 2.5(5)$ h. This is sufficient for the needs of experiments searching for a permanent electric dipole moment in ^{129}Xe. An integrated electric field sensor has been constructed which is coupled to a light source and light detectors via optical fibers. The sensor head does not contain any electrically conducting material.

1 Introduction

The observation of permanent electric dipole moments (EDMs) in elementary particles, atoms, and molecules could provide hints towards physics beyond the Standard Model of particle physics [1, 2]. A considerable number of experiments to search for EDMs are currently underway in several independent experiments, which employ different sample materials. They have in common that in each case, the sample is exposed to electric fields.

For all these modern precision experiments [3–6], knowledge of the strength of a static electric field inside the respective fiducial volume is, therefore, pivotal, because the final achievable accuracy and the reliability of the measured results depend linearly on the electric field and on the degree to which this field can be controlled and monitored. Typical methods employed in experiments to date include measurement and monitoring of a voltage difference applied between two conductive plates. Such a setup generates unavoidably a small current that flows between the electrodes which causes a small inhomogeneous magnetic field, i.e., magnetic field gradients which spoil the required magnetic field homogeneity in the fiducial volume. Alternately, in some cases, spectroscopic measurements of, e.g., stark shifts of spectral lines, can be observed to obtain the electric field strength inside a fiducial volume [7]. Such methods are difficult or even impossible to apply in several of the EDM experiments, which are presently underway. We report here on the measurement of static electric fields inside a closed glass measurement cell placed inside the field of an external electrode system as well as on the development of an electro-optic field sensor based on a $LiNbO_3$ crystal in the context of an EDM search on ^{129}Xe atoms [8, 9]. The sensor provides for reliably measuring and continuously monitoring a static electric field during periods of several hours. This time scale significantly exceeds the range of operation for commercially available devices[1] as well as that of laboratory setups which have been reported to date (see, e.g., [10–12]).

✉ K. Jungmann
k.h.k.j.jungmann@rug.nl

1 Van Swinderen Institute, University of Groningen, Groningen, The Netherlands

2 Nikhef Collaboration, Amsterdam, The Netherlands

3 Physikalisches Institut, Universität Heidelberg, Heidelberg, Germany

4 Institut für Physik, Universität Mainz, Mainz, Germany

5 Peter Grünberg Institut, Forschungszentrum Jülich, Jülich, Germany

6 Present Address: Physics Department, Yale University, New Haven, USA

[1] A sensor for high-frequency electric fields working at 250 MHz to 7 GHz is available, e.g., from Agiltron, Woburn, MA 01801, USA.

Published online: 22 October 2019

2 Electro-optic crystal properties

The polarization of light, which passes through an electro-optic crystal, is modified depending on the applied electric field and the orientation of the principal axes of this crystal [13]. For electric field monitoring over rather long periods, also the temperature dependence of crystal parameters [14] is of crucial importance. We have specifically chosen a Y-cut Z-propagation $LiNbO_3$ crystal (obtained from VM-TIM GmbH, Jena, Germany) to keep the temperature dependence [15] of its electro-optic performance minimal.

In such a crystal, an externally applied electric field will eventually be compensated inside the material on slow time scale by the build-up of an internal crystal electric field, which results in a decrease of the induced electro-optic birefringence. The build-up of a polarization slowly balances the external electric field, and the internal electric field vanishes eventually. The associated time constant τ_c is proportional to the crystal material's specific conductivity G [14]. We have

$$\tau_c \propto \frac{\epsilon_e \epsilon_r}{G}, \tag{1}$$

where ϵ_e and ϵ_r are the vacuum and relative material permittivities, respectively. With an external electric field applied as an instantaneous step function at $t = 0$, the internal electric field exhibits exponential behaviour thereafter, that is

$$E_{\text{crystal}}(t) = E_{\text{crystal}}(0) e^{-t/\tau_c}, \tag{2}$$

where $E_{\text{crystal}}(0)$ is the internal electric field induced at $t = 0$.

DC-field measurements require, therefore, a material with a rather long-time constant τ_c. Among the electro-optic crystals which are most suitable for DC measurements are lithium niobate ($LiNbO_3$) and bismuth germanate ($Bi_4Ge_3O_{12}$), for which the charge relaxation constants have been estimated to be 7×10^7 s and 248 s, respectively [16].

With no external electric field applied and in the absence of external or internal stress, lithium niobate is a uniaxial crystal. The index ellipsoid in the principal coordinate system is [13]

$$\frac{x_1^2}{n_1^2} + \frac{x_2^2}{n_2^2} + \frac{x_3^2}{n_3^2} = 1, \tag{3}$$

where $n_1 = n_2 = n_o$, $n_3 = n_e$ are the ordinary and extraordinary indices of refraction, and x_1, x_2 and x_3 are the optical axes. In an external electric field E, the index ellipsoid transforms into

$$\begin{aligned} &\left(\frac{1}{n_o^2} - r_{22}E_2 + r_{13}E_3\right)x_1^2 + \left(\frac{1}{n_o^2} + r_{22}E_2 + r_{13}E_3\right)x_2^2 \\ &+ \left(\frac{1}{n_o^2} + r_{33}E_3\right)x_3^2 + 2x_2x_3r_{51}E_2 + 2x_1x_3r_{51}E_1 \\ &- 2x_1x_2r_{22}E_1 = 1, \end{aligned} \tag{4}$$

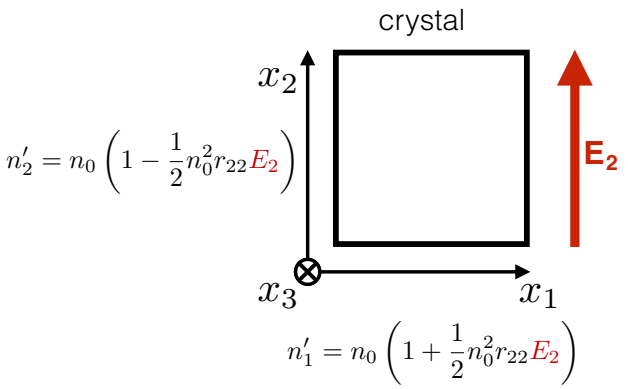

Fig. 1 Two principal axes of an electro-optic lithium niobate ($LiNbO_3$) crystal for the case of an electric field E_2 applied along the axis x_2. Light is in our case propagating along axis x_3

where r_{ij} are material dependent electro-optic coefficients.

Polarized light propagating along the crystal axis x_3 with an applied external electric field E_2 parallel to axis x_2 experiences the refractive indices in the principal coordinate system (see Fig. 1):

$$n_1' = \frac{1 - n_0^2 r_{22}\sqrt{E_1^2 + E_2^2}}{n_0^2}, \quad n_2' = \frac{1 + n_0^2 r_{22}\sqrt{E_1^2 + E_2^2}}{n_0^2}. \tag{5}$$

Here, n_1', n_2' are the refractive indices in the principal coordinate system x_1', x_2', which is rotated by an angle θ with respect to the principal coordinate system in zero external applied electric field (crystal axes x_1, x_2). The rotation angle θ in the x_1x_2 plane is

$$\theta = \frac{\pi/2 - \phi}{2}, \tag{6}$$

where ϕ accounts for an angle of the externally applied electric field with the axis to x_1 in the x_1x_2 plane. The birefringence as a function of the applied electric field is

$$\Delta n = -n_0^3 r_{22} E_{12}, \tag{7}$$

with E_{12} the magnitude of the electric field in the x_1x_2 plane, i.e., the birefringence depends in the chosen geometry only on the crystal-dependent electro-optic coefficient r_{22} and the external electric field.

The phase retardation in an electric field E_{12} is given by

$$\Gamma = \frac{2\pi \Delta n L}{\lambda} = -\frac{2\pi L n_0^3 r_{22} E_{12}}{\lambda}, \tag{8}$$

where L is the path length of light through the crystal and λ the light's wavelength.

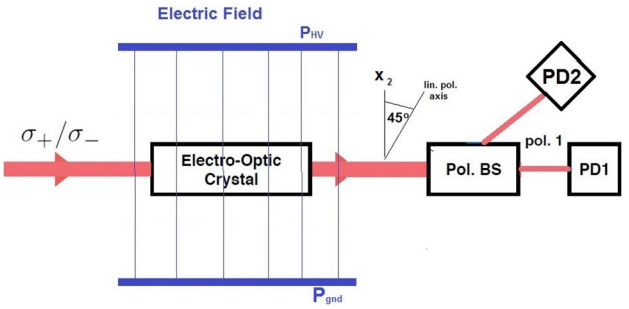

Fig. 2 Elliptically polarized light beam is created by laser light passing through a linear polarizer and a quarter-wave plate ($\lambda/4$). It travels through the electro-optic crystal (Y-cut Z-propagation $LiNbO_3$). The electric field between two large electrodes is applied along the crystal axis x_2. The beam exiting the crystal is decomposed into two orthogonal linearly polarized components with a polarizing beam splitter cube, the polarization axis of which is rotated by 45° with respect to the crystal axis x_2. Their intensities I_1 and I_2 are measured with the photo-diodes PD_1 and PD_2

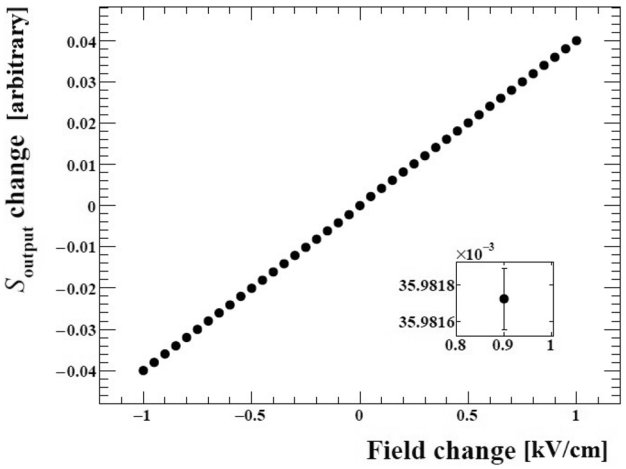

Fig. 3 Response to an external electric field change for a $LiNbO_3$ crystal (Y-cut Z-propagation). The electric field is ramped between − 1 and + 1 kV/cm in square steps of 50 V/cm every 6 s. The obtained resolution for electric field measurements is $\delta E > 4(1)$ V/cm (the insert shows an example of a data point at an enlarged scale)

3 Electro-optic electric field measurement

3.1 Experimental setup

We employed a $LiNbO_3$ crystal for measuring DC electric fields. In our setup, this crystal was mounted in the center between two parallel 12 cm × 40 cm metal plates which had 12 cm spacing and where the fringe field was shielded by 11 equidistant 5 mm diameter metal rods held at equidistant potentials by means of a resistive voltage divider. While one plate P_{gnd} was kept at ground potential, voltages in the range $-10\,\text{kV} < U_{HV} < +10\,\text{kV}$ could be applied to the second plate P_{HV} from a computer controlled high voltage power supply.

The $LiNbO_3$ crystal in our experiments had dimensions $x_1 = 5\,\text{mm} \times x_2 = 10\,\text{mm} \times x_3 = 25\,\text{mm}$, where x_2 was oriented along the external electric field. All six surfaces of the crystal were cleaned with ethanol and with acetone prior to our experiments. A light beam from a diode laser at wavelength 650 nm had diameter 2 mm and passed through a linear polarizer and a quarter-wave plate, the slow axis of which had an angle Θ with the polarizer axis. The laser light beam thereafter passed through the crystal along its axis x_3 and the Θ was adjusted to produce circular polarized light exiting the crystal. In our measurements, the laser light had intensity up to $I_0 < 50\,\mu\text{W/cm}^2$. The exiting light was decomposed into two orthogonal linear polarized components using a polarizing beam splitter cube under 45° with respect to the crystal axis x_2. The intensities I_1 and I_2 of the two components yield a measure for an applied electric field E parallel x_2 (see Fig. 2).

Neglecting light losses due to spurious absorption and surface reflections, we have

$$I_1 = \frac{1}{2}\left(1 - \frac{2\pi}{\lambda} n_0^3 r_{22} E\right) \quad \text{and} \quad I_1 = \frac{1}{2}\left(1 + \frac{2\pi}{\lambda} n_0^3 r_{22} E\right), \tag{9}$$

with $I_1 + I_2 = I$.

I_1 and I_2 are determined with two photo-diodes PD_1 and PD_2 (see Fig. 2) yielding the voltages U_{PD1} and U_{PD2}, respectively. The signal S, which is defined as

$$S = \frac{a_1(U_{PD1} - c_1) - a_2(U_{PD2} - c_2)}{a_1(U_{PD1} - c_1) + a_2(U_{PD2} - c_2)} \propto E, \tag{10}$$

where a_1 and a_2 are calibration constants and c_1 and c_2 are offsets for the photo-diode voltages, is proportional to the externally applied electric field E. Without crystal in the setup, the constants a_i and c_i $(i = 1, 2)$ can be balanced by adjusting the offsets and gains of the amplified photo-diode signals to achieve $c_1 = c_2 = 0$ and $a_1 = a_2$. The diode signals as well as the temperature near the setup were digitized every 1 s and this data was stored for analysis.

3.2 Crystal response to DC external electric fields

When stepping the electric field E between − 1 and + 1 kV/cm with 50 V/cm increment every 6 s, we observe a linear dependence of S on E (see Fig. 3). We find that changes in E can be resolved for steps $\delta E > 4(1)$ V/cm within 5 s averaging. The phase retardation in the crystal extracted from our data is 64 µrad cm/V over this range of electric fields.

To study the behaviour on long-time scales, we observed the signal S for constant voltages applied to the electrodes as function of time. For this, we periodically switched the high voltage U_{HV} on plate P_{HV} between 0 and $U_{HV} = 7800$ V to obtain DC electric fields E_{DC} between 0 and 640 V/cm. The lengths of the periods were between 5 and 14, 400 s. A sample signal of the of the crystal response S over a period

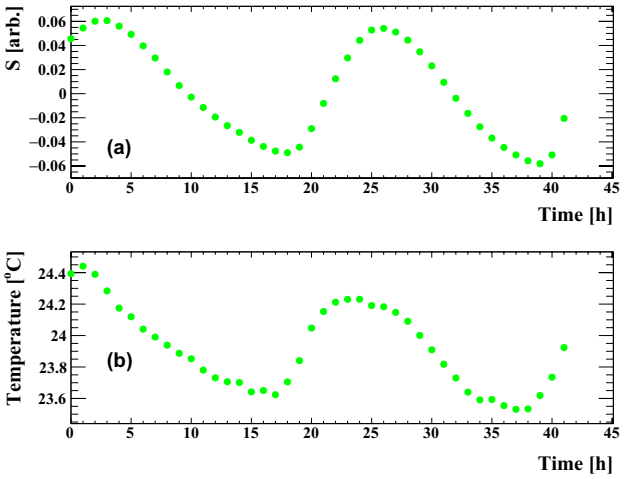

Fig. 4 Recording of electric field sensor signals in air averaged over 1 h periods (**a**) and the ambient temperature (**b**) over a period of 45 h. During every 1 h period, a constant electric field was applied externally to the crystal for 0.5 h, and thereafter, it was turned off for 0.5 h. Environmental temperature changes caused a correlated variation of the signal S. The effect has been exaggerated by allowing for rather large temperature fluctuations

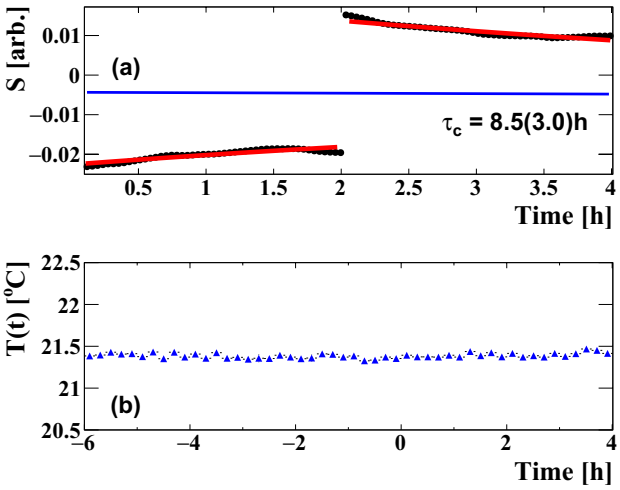

Fig. 5 **a** Data sample (black dots) for a $LiNbO_3$ crystal in laboratory air recorded for 4 h with a step function electric field change at $T = 0$ and at $T = 2$ h. The function (red line) in Eq. (11) was fitted simultaneously to two sections ($t < 2$ h and $t > 2$ h) of the data set. The linear term (blue solid line) representing the temperature drift is shown here separately, in addition to the full fit. **b** The temperature recorded in the proximity of the setup dropped by some 0.2 °C over the full time span from 6 h prior until the end of the actual electric field measurement

of 41 h is displayed in Fig. 4 together with the simultaneously measured environmental temperature T which has been chosen to demonstrate the effect in absence of an external electric field. A correlation between signal S and temperature T is visible, and a time shift t_o between both signals is apparent. Temperature measurement and control is, therefore, important for long-term field measurements. For this we passively stabilized the temperature of our setup to better 0.2 °C.

3.3 Modeling of the signal

For precise electric field determinations, we need to consider and include polarization decay in the $LiNbO_3$ crystal and temperature effects. The response of the electro-optic signal from the crystal (see Eq. (10)), which is exposed to a step function change in the external electric field, exhibits an exponential decrease of the output signal due to a slow buildup of polarization inside the material, which can be described by the time constant τ_c [see Eq. (1)].

The coefficient r_{22} has a residual dependence on temperature, which appears as a time-dependent offset in our data (see Fig. 4). This effect can be approximated by a linear function of time t by a linear coefficient α_T for every data set. We note that no further dependence on environmental parameters such as atmospheric pressure, air humidity, and exposure to ambient light could be observed. We find no influence of the laser light intensity up to 100 μW/cm^2.

The time-dependent sensor response $S(t)$ to a step function change in the external electric field at $t = 0$ can be modeled with an exponentially decaying part and the parametrized time behaviour of the temperature dependence of the birefringence in the crystal as

$$S(t) = S(0) \cdot \exp -t/\tau_c + \alpha_T \cdot (T_0 - T(t - t_o)). \quad (11)$$

Here, the coefficient α_T describes the influence of temperature $T(t)$ on the birefringence of the crystal and it is proportional to $\sin(\phi)$ with ϕ the angle between the crystal axis x_3 and the propagation direction of the light. By alignment, α_T can be minimized, and in general, its value needs to be determined (calibrated) for every particular crystal and chosen optical alignment. T_0 is the temperature when the setup was calibrated such that $\alpha_T \cdot T_0$ is known; t_o accounts for a time shift in the temperature measurement caused by the temperature sensor being located slightly outside the fiducial volume. For extracting τ_c from measurements using Eq. (11), the temperature of the crystal needs to be controlled sufficiently. We typically kept temperature variation below $\Delta T < 0.1$ °C for our reported measurements.

We fitted function (11) to our recorded data and we achieved good agreement. Figure 5 displays a data sample obtained with the crystal between the electrodes in air. Averaging the extracted values for τ_c, we obtain $\tau_c^{air} = 8.5(3.0)$ h for our $LiNbO_3$ crystal in the air.

The crystal responds to a sinusoidally modulated applied electric field at frequency $\omega_m/(2\pi)$ with a sinusoidal optical signal S at the same frequency, the phase of which is shifted by

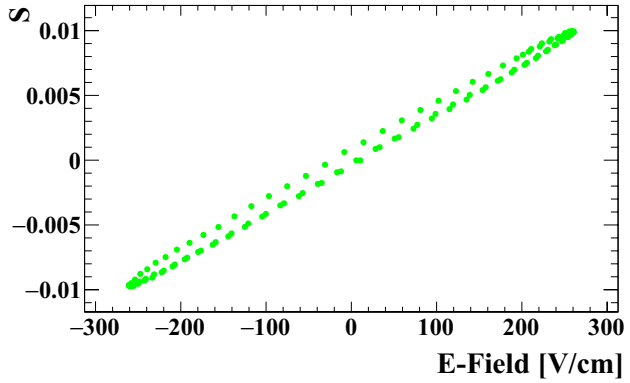

Fig. 6 Sample of a phase shift measurement between a sinusoidal electric field with a period of 3600 s applied to the $LiNbO_3$ crystal in Xe/He gas mixture (see also Fig. 10) and the electro-optic response S over a period of 1 h. The phase shift of 85(5) mrad between both signals yields $\tau_c^{\phi} = 1.9(1)$ h

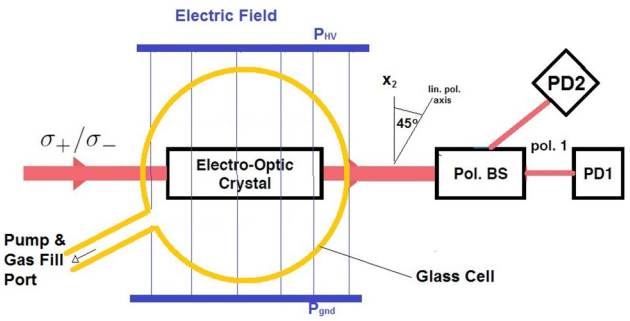

Fig. 7 Modified setup from Fig. 2. The $LiNbO_3$ crystal is centered in a spherical glass bulb which can be evacuated and filled with different gases

$$\phi_c(\omega_m) = \arctan\left(1/(\omega_m \cdot \tau_c^{\phi})\right). \quad (12)$$

In independent measurements, we determined $\phi_c(\omega_m)$ for several points in the range $1/100\,s^{-1} > \omega_m/(2\pi) > 1/7200\,s^{-1}$. Figure 6 displays a sample of such data. It enables extracting τ_c with an independent at τ_c^{ϕ} as 1.9(1) h. The value which we obtained is consistent with the result from a fit to the time-dependent function $S(t)$, where we find 2.0(1) h.

3.4 Electric field inside a closed glass container

In an experiment to search for a permanent electric dipole moment (EDM) on ^{129}Xe atoms [8], a spherical glass container holds spin polarized gases of 100 mbar ^{129}Xe and 25 mbar ^{3}He at room temperature. The glass cell is suspended inside an external electric field E_{DC} which is provided between two parallel conducting plates (see Fig. 7) and inside a constant magnetic field B parallel to E_{DC}.

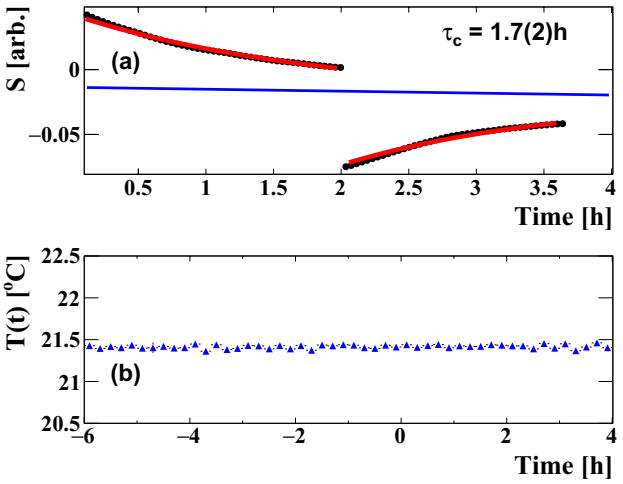

Fig. 8 **a** Data sample for a $LiNbO_3$ crystal inside a glass sphere filled with the air, recorded for 4 h with a step function electric field change at $T = 0$ and at $T = 2$ h. The function in Eq. (11) was fitted simultaneously to both sections of the data set. The linear term (blue solid line) is displayed separately as a solid blue line in addition to the full fit. **b** Temperature recorded close to the setup was stable to 0.1 °C over the full time span from 6 h prior until the end of the actual electric field measurement

The direction of E_{DC} is altered periodically to search for a signal from a potential EDM on ^{129}Xe atoms. For a reliable EDM result, one needs to know E_{DC} in the fiducial volume, i.e., inside the glass cell [8].

To study eventual electric field decay, we placed our crystal inside such a spherical cell of diameter 8 cm made from GE 180 material from Schott, Mainz, Germany. Its surfaces have been cleaned with ethanol and acetone prior to all measurements, and the cell remained untouched in the 6 week data collection period. We conducted measurements (1) where the cell had been filled with air (see Fig. 8), (2) where it had been evacuated to residual gas pressure below 3×10^{-3} mbar (see Fig. 9), and (3) where it had been filled with a Xe/He gas mixture at a similar partial pressure ratio as was employed in a ^{129}Xe EDM experiment (see Fig. 10). For all cases, the electric field was periodically switched between 0 and 640 V/cm every 2 h. The time behaviour can be described by Eq. (11) in all measurements.

Table 1 compiles the results of all our measurements. For the crystal exposed to the air in the laboratory between electric field plates, we find a time constant $\tau_c^T(\text{air}) = 8.5(3.0)$ h from fits to the exponential decay and $\tau_c^{\phi}(\text{air}) = 5.0(2.0)$ h from a phase shift analysis. These values average to $\tau_c(\text{air}) = 6.4(1.8)$ h. Inside a glass bulb containing Xe/He gas mixture, we have $\tau_c^T(\text{Xe/He}) = 2.0(1)$ h and $\tau_c^{\phi}(\text{Xe/He}) = 1.9(1)$ h, respectively (see Table 1). A conservative estimate of the influence of the glass cell on the electric field inside the glass bulb yields an electric field decay time constant:

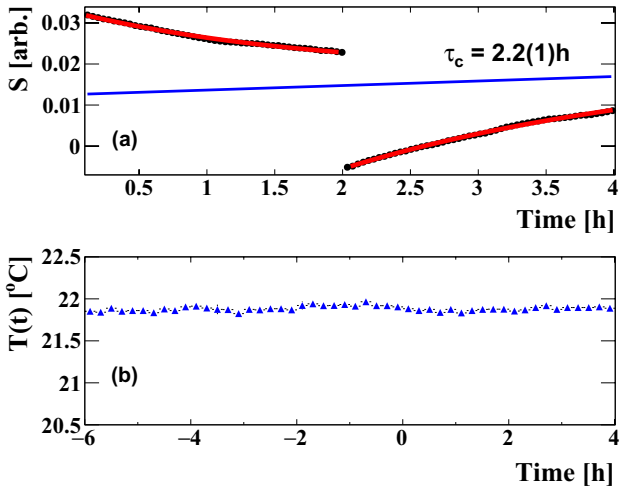

Fig. 9 **a** Data sample for a $LiNbO_3$ crystal inside an evacuated glass sphere recorded for 4 h with a step function electric field change at $T = 0$ and at $T = 2$ h. The function in Eq. (11) was fitted simultaneously to both sections of the data set. The linear term (blue solid line) is displayed separately as a solid blue line in addition to the full fit. **b** The temperature recorded close to the setup was stable to 0.1 °C over the full time span from 6 h prior until the end of the actual electric field measurement

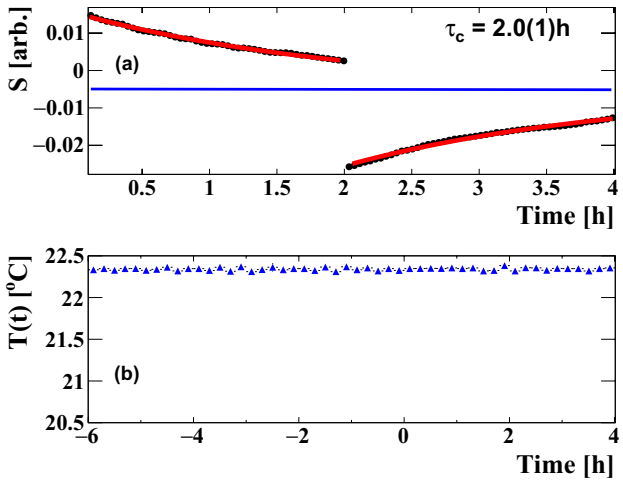

Fig. 10 **a** Data sample (black dots) for a $LiNbO_3$ crystal inside a glass sphere filled with 25 mbar He and 100 mbar Xe gas, recorded for 4 h with a step function electric field change at $T = 0$ and at $T = 2$ h. The function in Eq. (11) was fitted simultaneously to both sections of the data set. (red line). The linear term (blue solid line) representing the temperature drift is displayed separately as a solid blue line in addition to the full fit. **b** The temperature recorded close to the setup was stable to 0.1 °C over the full time span from 6 h prior until the end of the actual electric field measurement

$$\tau_E^{\text{glass}} = [1/\tau_c(\text{Xe/He}) - 1/\tau_c(\text{air})]^{-1} = 2.8(4)\,\text{h}. \tag{13}$$

For constant E^{ext} applied externally to a glass bulb at $t = 0$, we have the time-dependent field $E^{\text{ins}}(t)$ inside the glass envelope that acts on the crystal:

$$E^{\text{ins}}(t) = E^{\text{ext}} \cdot \exp(-t/\tau_E^{\text{glass}}). \tag{14}$$

From this, we estimate conservatively a lower bound on the average of the electric field inside a glass cell E^{ins} in a 2 h period of larger than 65% (at 90 % confidence level) of the applied external constant electric field E^{ext} at the beginning of the period.

In a separate and independent measurement series, we modified the setup, such that each of the two parallel electric field producing electrodes were touching the glass sphere on opposite sides. Mechanical contact was made over an area of $\approx$ 5 cm^2 for each of them. This could provide for a current path for eventual surface charges on the outside surface of the glass. We find within our uncertainty limits no significantly different time constants τ_c^T and τ_c^ϕ for both vacuum and a gas mixture of 25 mbar He and 100 mbar Xe gas in the cell .

We note that long-term monitoring of an electric field inside a glass cell for times t > 10 h is possible through exploiting the birefringence of $LiNbO_3$, provided the field strength at start ($t = 0$) exceeds 600 V/cm. The time constants for a bare crystal in air enables monitoring such fields for periods up to 1 day.

4 Integration into a compact sensor

4.1 Design of integrated compact sensor

Based on the laboratory measurements, a compact optical electric field measurement sensor system was designed [17]. It consists of a sensor head which receives light from either a laser or alternatively an LED light source through a single mode optical fiber (Thorlabs SM2000-custom) with 11(1) µm diameter core. To prevent environmental influences on the fiber changing the light's polarization, the circular polarization optics and the polarization decomposition optics are put next to the electro-optic crystal.

The light from the two orthogonal linearly polarized components exiting the crystal is focused onto one of two large bore optical fibers (Thorlabs FT1000EMT-custom) with 1000 µm diameter core, each. The light is transported via these fibers to two photo-detectors. By fixing all optical components after optimized alignment, the sensor's sensitivity to temperature can be minimized.

Apart from the optical components, the device is constructed from Macor material. All components are low magnetic noise. Figures 11 and 12 give a schematic and a photographic view on the integrated electro-optic sensor.

Table 1 Results from DC electric field determinations with a $LiNbO_3$ crystal

$LiNbO_3$ crystal in	Exp. decay τ_c^T (h)	Phase shift τ_c^ϕ (h)	Average τ_c (h)
Laboratory air glass cell	8.5 (3.0)	5.0 (2.0)	6.4 (1.8)
Filled with air	1.7 (2)	1.7 (1)	1.7 (1)
Under vacuum	2.2 (1)	1.9 (2)	2.1 (1)
Filled with Xe/He	2.0 (1)	1.9 (1)	2.0 (1)

For determining τ_c^T, the electric field was periodically switched between 0 and 640 V/cm every 2 h. The phase shifts are extracted from measurements with different periodicity. For the measurement in vacuum and in Xe/He gas mixture, the crystal was contained inside an electrically isolated glass container

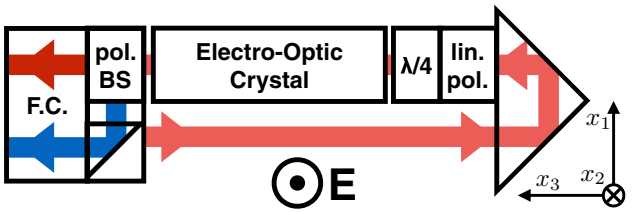

Fig. 11 Schematics of the integrated electro-optic field sensor. Light from a light source is transported via an optical fiber (not shown) and enters the assembly from the left, is collimated in a lens and reflected by a prism parallel to run parallel to the incoming beam. It is directed through a linear polarizer, a $\lambda/4$ plate and a $LiNbO_3$ crystal. The light exiting the crystal is decomposed into two orthogonal linear polarized components which are focused into an optical fiber each

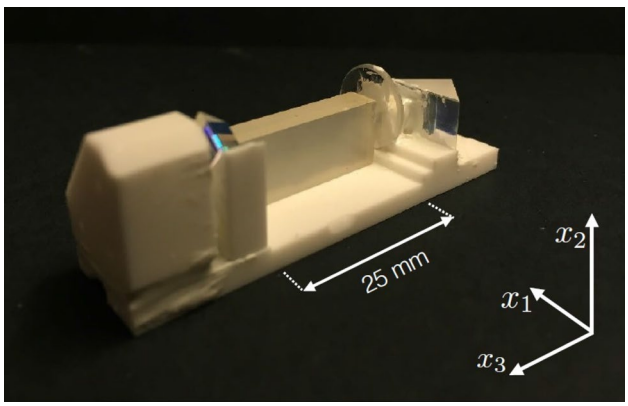

Fig. 12 Photograph of the integrated electro-optic electric field sensor. The optical fibers connecting to a light source and to two photodiodes are not shown. Those are attached to the holes visible on the left side of the Macor substrate

4.2 Performance test on the integrated sensor

We have performed measurements on the sensitivity of the integrated sensor using an LED source (Thorlabs M740F2). In our performance test experiments, the optical fibers were 20 m long. The sensor head had been mounted in the center of a homogeneous electric field volume between square electrodes of dimensions 10 cm × 8 cm which had 4 cm spacing. In these measurements, the crystal was aligned with its x_2

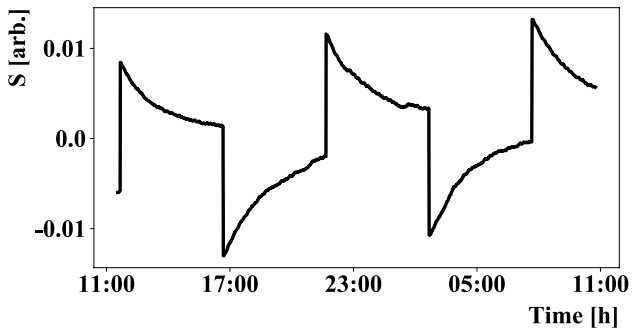

Fig. 13 Example of the response of the integrated sensor to an electric field which was externally applied in a step function. The electric field was switched between the states 0 V/cm and 1 kV/cm every 5 h. The signal decay time constant is $\tau_s = 1.7(1)$ h

-axis (see Fig. 12) parallel to the applied electric field. The integrated sensor has been tested in air. The signal which was obtained by regularly toggling the electric field between 0 and 1000 V/cm is displayed in Fig. 13. During the measurements, the temperature was stable within ± 0.2 °C. The signal shape is consistent with the signals from bare crystals. The extracted time constant $\tau_s = 1.7(1)$ h for its decay after a step function change of the electric field [17]. This result is in full agreement with the value extracted for a bare crystal (see Table 1). Figure 13 demonstrates that we can follow an electric field on the time scale of hours.

The signal-to-noise ratio for the integrated sensor operated with an LED light source is reduced compared to measurements using a bare crystal and more intense laser light. We find the sensitivity of the integrated sensor head to external fields to be 8(2) V/cm. Advantages of the integrated sensor are its compact design and its stable performance due to the light delivery to the sensor and the readout of the signal light by optical fibers. Sending unpolarized light from an LED light source to the sensor head makes the device insensitive to mechanical vibrations, or even significant movement of the optical fibers, as long as the sensor head remains stable in its position. This provides for long-time stable and vibration insensitive operation. Therefore, we have chosen to employ unpolarized LED light rather than polarized laser light to obtain stability of performance while operating the

integrated sensor. The device head can be placed at locations that are not directly accessible for free space laser beams. The sensor head reported here displays similar performance to a bare crystal operated with free space laser beams, and it exceeds the sensitivity to DC electric fields ($t > 1$ h) achieved in earlier approaches [10, 14, 16, 18].

5 Conclusion

An optical electric field sensor for DC electric fields has been developed. It is based on a Y-cut Z-propagation lithium niobate electro-optic crystal. The material's long-time constant τ_c enables field monitoring for several hours, provided that the environmental temperature can be sufficiently monitored or controlled. Since the response of the crystal to a step function external field change exhibits only exponential decay, deconvolution of a recorded arbitrary signal is straightforward and the time dependence of the external field can be obtained from this. A bare crystal placed into an external electric field read out with laser light propagating through free space has 4(1) V/cm resolution. We have built on this concept an all non-metallic sensor head which is coupled to a light source and photo-detectors by means of optical fibers. Such a sensor head is non-conductive due to material selection and it also has low magnetic noise. A sensitivity to external electric fields of 8(2) V/cm was achieved. The integrated sensor can be employed, where next to electric fields also magnetic fields are crucial.

Acknowledgements The authors owe their thanks O. B oll and L. Huisman for technical support, and F. Allmendinger, W. Heil and U. Schmidt for their constant interest and fruitful discussions.

Funding Klaus Jungmann, Olivier Grasdijk and Lorenz Willmann were funded through the research programme Broken Mirrors and Drifting Constants with project number FOM 125, which is nanced by the Dutch Research Council (NWO).

References

1. K. Jungmann, Ann. Phys. **525**(8–9), 550 (2013). https://doi.org/10.1002/andp.201300071. https://onlinelibrary.wiley.com/doi/abs/10.1002/andp.201300071
2. L. Willmann, K. Jungmann, Ann. Phys. **528**(1–2), 108 (2016). https://doi.org/10.1002/andp.201500008. https://onlinelibrary.wiley.com/doi/abs/10.1002/andp.201500008
3. B. Graner, Y. Chen, E.G. Lindahl, B.R. Heckel, Phys. Rev. Lett. **116**, 161601 (2016). https://doi.org/10.1103/PhysRevLett.116.161601. https://link.aps.org/doi/10.1103/PhysRevLett.116.161601
4. V. Andreev, D.G. Ang, D. DeMille, J.M. Doyle, G. Gabrielse, J. Haefner, N.R. Hutzler, Z. Lasner, C. Meisenhelder, B.R. O'Leary, C.D. Panda, A.D. West, E.P. West, X. Wu, A. Collaboration, Nature **562**, 355 (2018). https://doi.org/10.1038/s41586-018-0599-8
5. T. Chupp, M. Ramsey-Musolf, Phys. Rev. C **91**, 3 (2015). https://doi.org/10.1103/PhysRevC.91.035502
6. B.M. Roberts, V.A. Dzuba, V.V. Flambaum, in *Annual Review of Nuclear and Particle Science*, vol. 65, ed. by B. Holstein, pp. 63–86 (2015). https://doi.org/10.1146/annurev-nucl-102014-022331
7. H. Ashworth, Towards an improved measurement of the electron electric dipole moment. Ph.D. thesis, Imperial College London (2009)
8. F. Allmendinger, I. Engin, J.O. Grasdijk, W. Heil, K. Jungmann, S. Karpuk, H.J. Krause, B. Niederländer, A. Offenhäusser, M. Repetto, U. Schmidt, L. Willmann, S. Zimmer, Proceedings zur PPNS 2018, Grenoble (2019)
9. F. Allmendinger, I. Engin, W. Heil, S. Karpuk, H.J. Krause, B. Niederländer, A. Offenhäusser, M. Repetto, U. Schmidt, S. Zimmer, Phys. Rev. A **100**, 022505 (2019). https://doi.org/10.1103/PhysRevA.100.022505. https://link.aps.org/doi/10.1103/PhysRevA.100.022505
10. M. Bordovsky, Electrooptic electric field sensor for dc and extra-low-frequency measurement. Ph.D. thesis, Brunel University School of Engineering and Design (1998)
11. C. Gutierrez-Martinez, R. Ricardez-Trejo, Appl. Opt. **57**(32), 9677 (2018). https://doi.org/10.1364/AO.57.009677. http://ao.osa.org/abstract.cfm?URI=ao-57-32-9677
12. B. He, S. Liu, P. Zhu, Y. Li, D. Cui, Meas. Sci. Technol. **29**(12), 125004 (2018). http://stacks.iop.org/0957-0233/29/i=12/a=125004
13. B.E.A. Saleh, M.C. Teich, *Fundamentals of photonics*, 2nd ed. Wiley Series in Pure and Applied Optics (Wiley, New York, 2007)
14. F. Cecelja, W. Balachandran, IEEE Trans. Instrum. Meas. **51**(4), 866 (2002). https://doi.org/10.1109/TIM.2002.803512
15. K. Takizawa, L. Jin, Opt. Rev. **18**(2), 203 (2011). https://doi.org/10.1007/s10043-011-0043-x
16. F. Cecelja, M. Bordovsky, W. Balachandran, IEEE Trans. Instrum. Meas. **51**(2), 282 (2002). https://doi.org/10.1109/19.997825
17. J.O. Grasdijk, Search for the Permanent Electric Dipole Moment of ^{129}Xe. Ph.D. thesis, University of Groningen (2017)
18. F. Cecelja, M. Bordovsky, W. Balachandran, IEEE Trans. Instrum. Meas. **50**(2), 465 (2001). https://doi.org/10.1109/19.918167